# Large Workspace Haptic Devices - A New Actuation Approach

Michael Zinn*
Department of Mechanical Engineering
University of Wisconsin - Madison

Oussama Khatib†
Robotics Laboratory
Department of Computer Science
Stanford University

Bernard Roth‡
Design Division
Dept. of Mechanical Engineering
Stanford University

J. Kenneth Salisbury§
Robotics Laboratory
Dept. of Computer Science
Stanford University

## ABSTRACT

Large workspace haptic devices have unique requirements, requiring increased power capabilities along with increased safety considerations. While there are numerous haptic devices available, large workspace systems are hampered by the limitations of current actuation technology. To address this, the Distributed Macro-Mini ($DM^2$) actuation method has been applied to the design of a large workspace haptic device. In this paper, the $DM^2$ method and present experimental results which demonstrate its effectiveness. Finally, the control design is presented along with a discussion of the unique challenges associated with its robustness.

## 1 INTRODUCTION

Large workspace haptic devices have a unique set of requirements. These include similar requirements which bound traditional desktop devices as well as additional power and force requirements which can be very demanding. A number of researchers have developed device performance and requirement guidelines [5, 10, 12]. These, in combination with the additional power and safety requirements for large workspace devices, can be summarized as follows:

**Large dynamic range force control:** To accurately render a virtual object, a haptic device must have the capability to render forces over a large dynamic range, in both frequency and magnitude. This requirement can be partitioned as follows:

> **Torque Vs. Frequency:** As shown in [21], as well as elsewhere, the required force output for many devices, including haptic devices, is inversely proportional to frequency ($1/\omega$) while power magnitude is inversely proportional to the square of frequency ($1/\omega^2$). At low frequencies, large forces are required to react DC or slowing changing forces, such as would be expected when pressing into a virtual object. At high frequencies, brief instances of high frequency force content are required to render stiff surfaces (e.g. during contact transitions). While these forces are often short in duration and low power, their presence is critical for the accurate rendering of stiff objects.
>
> **High Bandwidth:** While required torque and power magnitude falls off with increased frequency, small amplitude actuator torques must be capable of supporting a high bandwidth system. This is important to prevent excessive distortion of the rendered forces. In the case of admittance devices with a given closed-loop bandwidth, $\omega_{CL}$, the actuator torque output must not introduce phase distortion at frequencies below $\omega_{CL}$.

*e-mail: mzinn@wisc.edu
†e-mail:ok@robotics.stanford.edu
‡e-mail:roth@robotics.stanford.edu
§e-mail:jks@robotics.stanford.edu

**Transparency:** An important characteristic of a haptic device is the ability to display zero force over a wide frequency range. Introduction of device friction, inertial, or control forces which deviate from this ideal reduce the effectiveness of the device. This requirement can be further broken down by frequency range:

> **High frequency - *Low effective inertia:*** Regardless of the architecture of the haptic device (i.e. admittance vs impedance), at high frequencies the transparency is dominated by the effective inertia of the device. The effective inertia is, in turn, affected by the mass properties of the mechanism, the reflected inertia of the actuation, and location within the device workspace. In the case of admittance devices, the effective inertia is dominant above the closed-loop bandwidth of the admittance controller. For good transparency at high frequencies, the physical device must possess low effective inertia.
>
> **Low frequency - *Low output impedance:*** At lower frequencies, the transparency of a device is affected by its frictional characteristics and, to a lesser extent, by its mass properties. For impedance devices, it is important to keep the effective friction forces low. Friction sources include actuation gear-train and joint friction. The low frequency output impedance of admittance devices is determined by its controller design and implementation in combination with the physical characteristics mentioned above.

**High power / large force:** In addition to those requirements listed above, a large workspace imposes the additional requirements of high force and power. A major purpose of a large workspace device is to allow full arm or body haptic interaction. This type of task involves higher forces than devices which are designed for desktop use. The larger force, in combination with the larger workspace, implies larger work and power output. It is this requirement, in combination with transparency and force control requirements, which make the design of large workspace haptic devices so challenging.

**Safety:** With the increased torque and power capabilities of a large workspace haptic device comes a new requirement of safety. Device safety is dependent on its mechanical, electrical, and software design characteristics. However, the biggest danger present when working in close proximity with a high power device is the potential for large impact loads resulting from the large effective inertia. To insure a minimal level of safety, a large workspace haptic device should be designed to minimize its effective inertia [20, 21].

Numerous kinesthetic haptic devices have been successfully designed, including a number which have had commercial success [2, 9, 6]. Most devices have been developed for desktop use, with only a few applicable to large workspace applications [18, 1, 6, 19]. While there has been some limited success in developing larger workspace devices, these systems, in general, have been hampered by performance limitations (in the case of impedance devices) or safety concerns (in the case of admittance

devices). It is our belief that the limitation of current actuation methods is the primary obstacle in the development of high-performance large workspace haptic devices. In the following sections, we will present a new actuator concept which addresses the requirements enumerated above, allowing for the design of a haptic device with the ability to render stiff environments over a large workspace. Experimental data shall be presented which demonstrates the effectiveness of the new method.

## 2 Distributed Macro-Mini Actuation Approach

A new actuation approach, referred to as the distributed macro-mini actuation approach ($DM^2$), has been developed to overcome the limitations that traditional actuation methods. The unique characteristics of the $DM^2$ approach make it well suited for large workspace haptic devices. The overall approach is shown in Fig. 1

The first part of the $DM^2$ actuation approach is to divide the torque generation into separate low and high-frequency actuators whose torque sum in parallel. The partitioning of torques is motivated by the torque vs frequency requirement described in Section 1. A high-power, high-torque actuator is used to provide the low frequency torques while a small, fast actuator is used to provide the high frequency torques.

The second part of the $DM^2$ actuation approach is to distribute the low and high-frequency actuators to locations on the device where their effect on device transparency is minimized while their contribution to force dynamic range is maximized. This is achieved by locating the low-frequency actuator remotely from the actuated joint. This is particularly advantageous as the low frequency components of most haptic device force profiles are considerably larger in magnitude than the high frequency components, and consequently require a relatively large actuator. To maintain high-bandwidth, the high-frequency actuator is collocated with the joint to allow undistorted transmission of high frequency torque content. While a number of researchers have explored parallel actuation approaches [11, 13, 21] the concept of actuator distribution and its application to the development of haptic devices has not been explored. Finally, to provide decoupling between the low and high-frequency actuators and to improve the low frequency output impedance, a Series Elastic Actuator [15] is utilized for the base actuator. The SEA actuator incorporates an elastic coupling at its output which, in combination with local torque feedback, decouples the low and high-frequency actuators and dramatically reduces the output impedance of the low-frequency actuator over a broad frequency range [16].

### 2.1 $DM^2$ Specifications

The effectiveness of the $DM^2$ approach can be evaluated against the actuator requirements summarized in Section 1. The following sections will address each of these requirements in turn.

#### 2.1.1 Torque Vs. Frequency

High performance tasks require actuation torque over a broad range of frequencies. As shown in Section 1, actuator torque requirements as a function of frequency are proportional to $1/\omega$ where $\omega$ is the operating frequency. The $DM^2$ actuation approach satisfies this requirement by combining a large low-frequency actuator with a small high-frequency actuator in parallel.

The low-frequency actuation is designed to have high torque and power output. Its location off of the manipulator allows for heavier, higher power actuator. Drive-train compliance between the low-frequency actuator and driven joint is not of concern as it is required to transmit low frequency torques only. High frequency torques are provided by small servo motors collocated at the joint. Because the high-frequency actuator produces torque intermittently, consisting of only high frequency components, it can be used much closer to their peak current limits. A simple thermal model of the motor windings, with sufficient safety margin, is employed in software to prevent overheating of the high-frequency actuators.

The combination of the low and high-frequency actuators provides an output torque profile as a function of frequency that more closely matches the $1/\omega$ requirement discussed above. As seen in Figure 2, the two-axis prototype described in Section 4 benefited substantially from the combination of low and high-frequency actuators, producing a torque vs frequency profile which more closely matches the requirements of Section 1. While the low-frequency SEA actuator output torque falls off rapidly above it closed-loop bandwidth (2.0 Hertz), the addition of the high-frequency motor torque extends the torque envelope to higher frequencies.

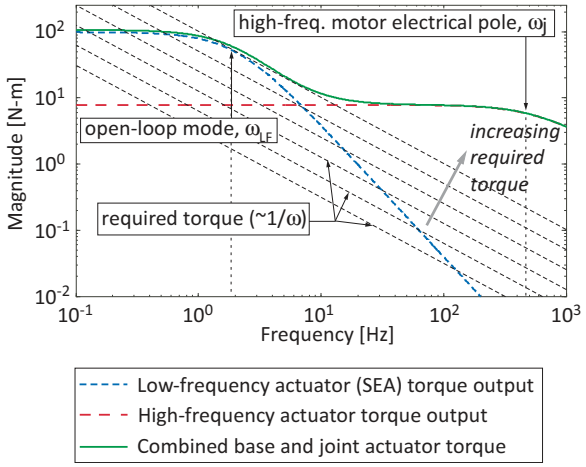


Figure 2: Maximum actuation torque output versus frequency.

#### 2.1.2 High Bandwidth

The primary obstacle to achieving high-bandwidth control is the introduction of dynamics between the actuation and driven-link. Examples of these unwanted dynamics include higher frequency actuator dynamics, such as the electrical winding dynamics, drive-train backlash, friction, and, most troublesome, drive-train compliance. The key to achieving high bandwidth is the elimination of these characteristics.

The $DM^2$'s distributed actuator approach, as well as the proper selection of actuator and gearing, eliminates the unwanted dynamics described above. The use of low inductance servo motors guarantees that the electrical time constant is sufficiently high so as to avoid interaction with the control loop. To avoid friction and backlash, the current embodiment of the $DM^2$ approach employs a cable gear-reducer design possessing very low friction levels and essentially zero backlash.

While these characteristics are important, the most essential element of the $DM^2$ approach is the collocation of the mini actuator with the manipulator joint. The closed-loop position-bandwidth is limited by the presence of compliance between the actuator and driven-link. More specifically, the maximum cross-over frequency, $\omega_c$, and, by inference the maximum bandwidth, is limited to approximately $1/5^{th}$ of the first mode frequency, $\omega_j$. By collocating the high-frequency actuator with the manipulator joint, the drive-train compliance can be minimized. Currently, $DM^2$ implementations have employed a single-stage cable gear reduction with specific stiffening design elements such as dual-cable drive, minimized free cable lengths, and rigid drive component supports. A cable gear reduction was chosen to minimize friction and maintain low output impedance. While these features are implementation specific, the objective is to create a high stiffness connection between

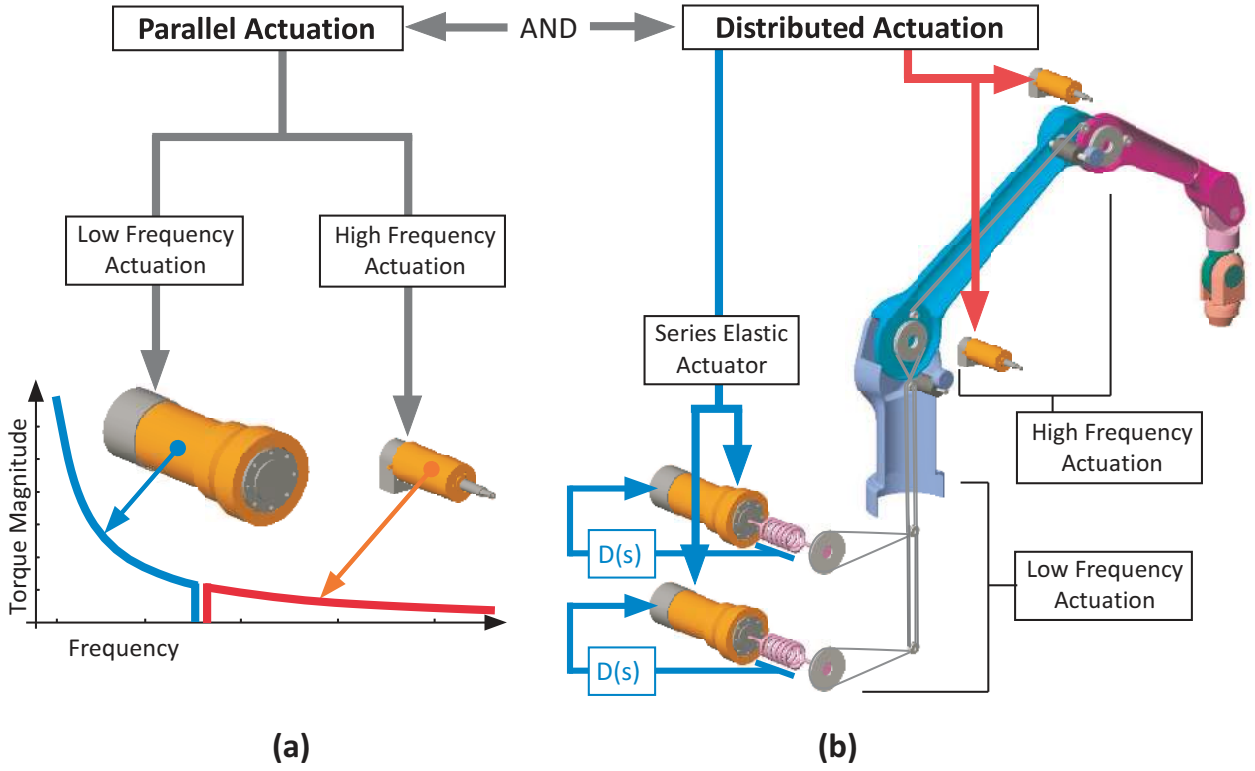


Figure 1: Distributed macro-mini actuation approach (DM$^2$) (**a**)Partition of torque into low and high frequency (parallel) components (**b**) Distributed actuation: Large, low-frequency actuators are located at base. Small, high-frequency actuators are located at the joints.

the high-frequency actuator and driven-link and, thereby, achieve the characteristics required for high bandwidth control.

### 2.1.3 Low Effective Inertia

For a given device, the effective inertia is a function of both the device's inertia as well as the reflected actuator inertia. The DM$^2$'s approach of placing the low-frequency actuator at the base has the beneficial effect of reducing both of these.

The reduction in the actuator reflected inertia is due to the decoupling of the actuator inertia from the device. This decoupling is due, primarily, to the elastic coupling placed between the large low-frequency actuator and the driven joint. When the compliance between the actuator and the link is low, the system acts as a low pass filter which isolates the actuator's reflected inertia from the device, reducing the effective inertia perceived by the user and insuring good device transparency (at frequencies above the first mode).

### 2.1.4 Low Output Impedance

The DM$^2$ approach uses the series elastic actuator method (SEA) [15] with the large, low-frequency actuator. Through a combination of mechanical compliance and closed-loop control, the SEA actuator can provide significant reduction in output impedance. At frequencies below the closed-loop bandwidth of the SEA controller, $\omega_s$, the reflected inertia is reduced by the square of the ratio of the natural frequency of the uncontrolled system, $\omega_n$, to $\omega_s$:

$$\left.\frac{\tau_s(s)}{\theta_a(s)}\right|_{s\to 0} = \frac{\omega_n^2}{\omega_s^2} I_{eff} \tag{1}$$

where $I_{eff}$ is the effective inertia of the actuator and gear train. This reduction can be quite large. In the case of the two axis prototype described in Section 4, the actuator and gear train reflected inertia was reduced by a factor of greater than ten.

Another contributor to output impedance is the inertia, $I_j$, and friction, $\tau_f$, of the high-frequency actuator. As measured at the joint, the output impedance is given as

$$\frac{\tau_j(s)}{\theta_a(s)} = N_j^2 I_j + N_j \tau_f \tag{2}$$

where $N_j$ is the high-frequency motor gear reduction. Both the inertia and friction component of the output impedance must be minimized. By design, the high-frequency actuator is selected to have low inertia, high peak torque and low inductance. The selection of a fast ironless core servo motor keeps the overall output impedance of the high-frequency actuator small. Because the motors can produce high peak torque in relation to their size, a high reduction transmission in not required, preventing the reflected output impedance from being excessively amplified through the gear reduction. The gear reduction friction is minimized through selection of designs, such as the use of a single stage cable transmission, which have very low friction characteristics while maintaining high stiffness between the actuator and the manipulator. In the case of the two-axis prototype described in Section 4, the reflected high-frequency actuator inertia, as measured at the joint, was less than $1/20^{th}$ of the link inertia.

Finally, the device structure can be a contributor to the output impedance, particularly for large workspace devices. While locating the large low–frequency actuators at the base of the manipulator structure was motivated primarily by the desire to reduce the effective inertia at the input, a consequence of this choice was a significant decrease in device output impedance at low frequency, as compared to a design whose primary power actuators are located on the structure itself. In the case of the two-axis prototype described in

section 4, the effective inertia for the proximal joint would increase by a factor of three if the low-frequency actuators were collocated with the manipulator joints.

#### 2.1.5 High Power - Large Forces

The distributed characteristic of the DM$^2$ approach is ideal for the application of large force and high power. At low frequencies, the size of the actuation input is virtually unconstrained because it does not significantly contribute to the device's effective inertia. At high frequencies, the power requirements are modest and can be easily handled by the high-frequency actuator collocated with the joint.

### 2.2 Safety:

As shown in [20], the potential for injury is governed by a device's effective inertia. The DM$^2$ approach, with its use of a SEA actuator along with the distribution of the parallel actuation, has been shown to dramatically reduce the effective inertia for a given device. The potential for injury, as measured by a new metric know as the Manipulator Safety Index (MSI), is reduced by more than an order of magnitude when compared to conventional actuation [20].

## 3 DM$^2$ Control Approach

The control approach seeks to leverage the characteristics of the parallel actuator structure while dealing with the control challenges associated with the use of low impedance actuation. At the joint level, the DM$^2$ approach is essentially a dual-input single-output system. The redundant actuators provide an additional degree of freedom which can be used in optimizing system performance while minimizing actuation effort. For example, in the case of trajectory tracking, we can use LQR control techniques to obtain an optimum control law based on minimizing control effort and tracking error. The low and high-frequency actuation effort partitioning can be accomplished in a similar manner. Recently, dual-actuator control approaches have been developed for applications in the disk-drive industry [17]. However, these types of control structure are specific to a given task, in this case to trajectory tracking, and do not provide a black-box interface to the actuation similar to the use of a single actuator. In particular, for applications involving a number of different control modes, such as free-space motion followed by contact transitions, or for applications requiring a low-impedance torque source, such as haptics or tele-robotic master devices, we desire an actuation control scheme which allows the use of the parallel actuation system as a single torque source.

The overall control approach seeks to exploit the DM$^2$ actuation's unique characteristic to construct a near perfect torque source. The characteristics of a perfect torque source, consisting of zero output impedance and infinite control bandwidth, are ideal for a haptic device. While a perfect torque source is impossible to achieve, a near perfect torque source, with low output impedance relative to the driving load and high bandwidth torque capability, offers much of the same advantages.

### 3.1 Single Joint Control Structure

For most haptic devices, the distributed structure of the DM$^2$ approach will result in a design whereby the low and high-frequency actuators do not map one-to-one to specific joint torques. Each joint torque will not be the sum of a single low and high-frequency actuator torque but rather, depending of the coupling of the transmission to joint motion, will be a linear combination of a subset of actuator torques. While this coupling exists, it is instructive to examine the structure and properties of the DM$^2$ control from the view point of a simple one-degree-of-freedom mechanism. The simple control structure of the DM$^2$ approach can be easily extended to a multi-dimensional framework[20]

#### 3.1.1 Combined Low and High-Frequency Actuator Control Structure

The DM$^2$ distributed design allows for the implementation of a straight-forward parallel actuator control structure. As seen in Figure 3, the desired DM$^2$ torque is commanded to the low-frequency SEA actuator. The low-frequency actuator error term is used as the command input to the high-frequency actuator. This simple topology is possible due to the low friction transmission between the low-frequency actuator and link. An alternative strategy of placing the low-frequency actuator compliance at the joint would provide the same functionality and would be immune to transmission friction torques. However, this implementation would severely limit the bandwidth of the low-frequency SEA actuator, requiring additional high-frequency actuator control authority and would limit the combined overall bandwidth.

A physical schematic of the control structure for a one-degree-of-freedom joint along with an equivalent block diagram representation are shown in Figures 3(a) and (b), respectively. The transfer function of the control structure shown in Figure 3(b) has unit gain and zero phase over all frequencies ($\frac{T_{actual}(s)}{T_{desired}(s)} = 1$). A simplified representation, shown in Figure 4, demonstrates how the control approach utilizes the low-frequency base actuator's low pass filter characteristics to partition the control torques into low and high frequency components.

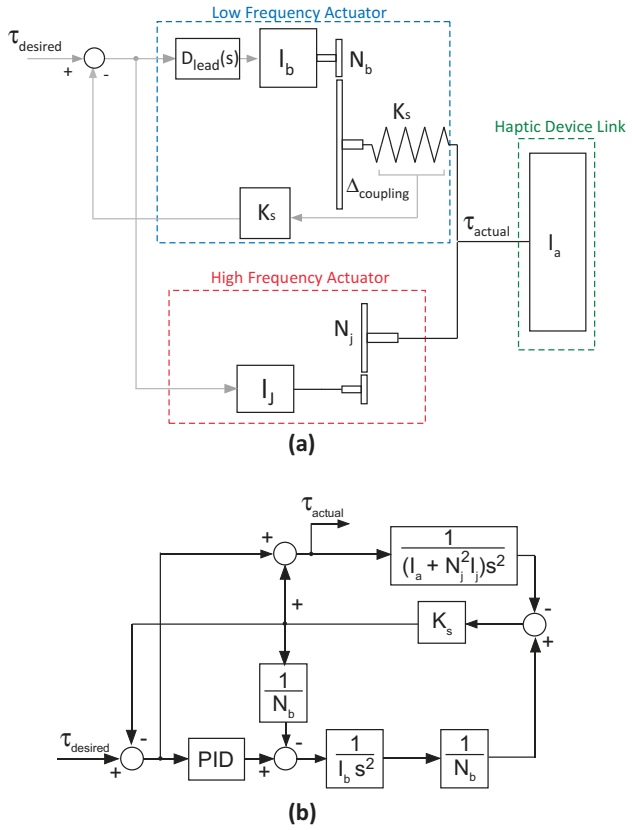


Figure 3: **(a)** DM$^2$ Actuation and control topology (single degree-of-freedom). **(b)** DM$^2$ Actuation and control block diagram representation (single degree-of-freedom). $\mathbf{I_a}$: device link inertia, $\mathbf{I_b}$: low-frequency actuator rotor inertia, $\mathbf{I_j}$: high-frequency actuator rotor inertia, $\mathbf{N_b}$: low-frequency actuator gear-ratio, $\mathbf{N_j}$: high-frequency actuator gear-ratio, $\mathbf{K_s}$: low-frequency actuator (SEA) compliance

By using the actual measured torque output from the low-

frequency actuators in combination with the desired torque, we automatically compensate for the non-ideal behavior of the low-frequency actuators. Assuming that the smaller high-frequency actuators can produce this torque, the combined torques sum is a perfect realization of the desired torque. The frequency partitioning can be clearly seen if we rearrange the structure in Figure 4a into a pure parallel structure, as shown in Figure 4b. As seen in Figure 4b, the low-frequency actuator's transfer function falls off above its closed-loop bandwidth, $w_{LF\,closed-loop}$, while the equivalent high-frequency actuator's transfer function approximates a double lead filter, which adds phase to the combined system above the open-loop mode frequency, $w_{LF}$, and attenuates the DC and low frequency components commanded to the high-frequency actuator.

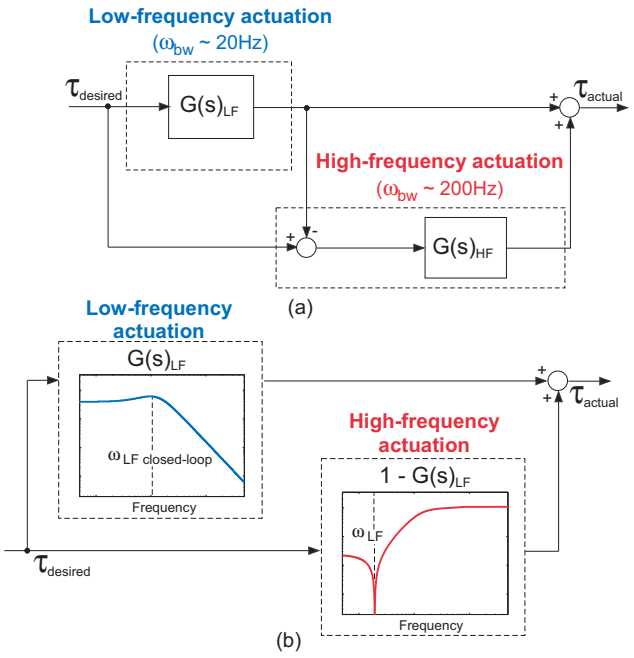


Figure 4: **(a)** DM$^2$ actuation control structure and **(b)** frequency response. $\mathbf{G(s)_{LF}}$: low-frequency actuator closed loop transfer function, $\mathbf{G(s)_{HF}}$: High-frequency actuator transfer function, $\omega_{\mathbf{LF}}$: open-loop natural frequency of low-frequency actuator, $\omega_{\mathbf{LF-closed-loop}}$: closed-loop bandwidth of low-frequency SEA controller

The combined actuator control structure creates a perfect torque source in the linear sense, where the torques sum to unit magnitude and zero phase, as seen in Figure 5a and 5b. Thus, by using the simple control structure describe above, we can create a unified actuator with the desirable characteristics of low impedance and high bandwidth torque controls.

### 3.2 Control Challenges

Perhaps the most challenging aspect of a DM$^2$ implementation is the development of a control approach which is robust to unmodeled system dynamics. While there are a number of specific challenges which must be addressed when using a DM$^2$ approach [20], the main challenge in implementing the control scheme comes primarily from high-frequency actuator drive-train compliance.

#### 3.2.1 Haptic Rendering With Low Impedance Actuation

While the high-frequency actuator usually has a relatively stiff single-stage transmission design, some level of compliance is unavoidable. The drive train compliance in combination with the low

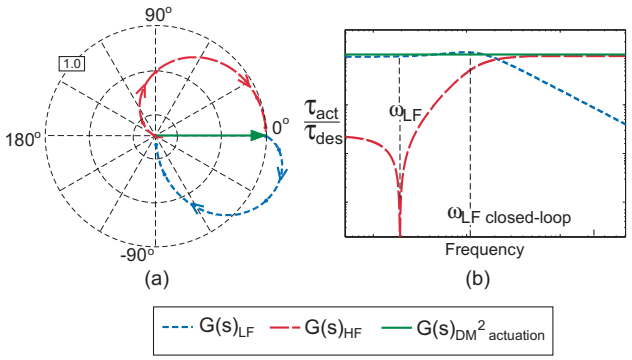


Figure 5: (**a**) Perfect torque source: Low-frequency, high-frequency, and combined DM$^2$ actuator torque magnitude vs phase polar plot (**b**) Near perfect torque source: Low-frequency, high-frequency, and combined DM$^2$ actuator torque magnitude vs frequency. $\mathbf{G(s)_{LF}}$: low-frequency actuator closed loop transfer function, $\mathbf{G(s)_{HF}}$: High-frequency actuator transfer function, $\mathbf{G(s)_{DM^2actuation}}$: Combined DM$^2$ actuator transfer function, $\omega_{\mathbf{LF}}$: open-loop natural frequency of low-frequency actuator, $\omega_{\mathbf{LF-closed-loop}}$: closed-loop bandwidth of low-frequency SEA controller

reflected inertia of the high-frequency actuator produces low frequency oscillations which can limit closed-loop performance.

We can more clearly understand this phenomenon using a simplified model of the DM$^2$ system that includes the drive train compliance but ignores the coupling with the low frequency base actuator. Figure 6a and Equation (3) show the assumed model and its uncompensated open-loop transfer function. This assumes collocation of the high-frequency motor and joint axis. Figure 6b and Equation (4) given the non-collocated case, which will be discussed in the next section.

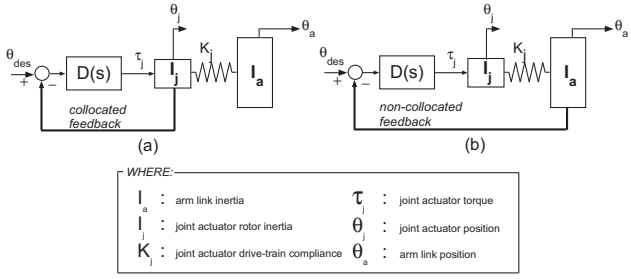


Figure 6: Spring-mass model of joint actuator and driven link inertias (**a**) Collocated control (**b**) Non-collocated control.

In many servo-systems, including those in haptics, the actuator and link inertias are matched or nearly matched to achieve optimum power and acceleration transfer from motor to load. In this situation, the poles and zeros of the transfer function, given by (5), are approximately equal in frequency.

$$\frac{\theta_j(s)}{\tau_j(s)} = \frac{s^2 I_a + K_j}{s^2(s^2 I_a I_j + K_j(I_a + I_j))} \tag{3}$$

$$\frac{\theta_a(s)}{\tau_j(s)} = \frac{K_j}{s^2(s^2 I_a I_j + K_j(I_a + I_j))} \tag{4}$$

$$\omega_{zero} = \sqrt{\frac{K_j}{I_a}} \quad \text{and} \quad \omega_{pole} = \sqrt{\frac{K_j(I_j + I_a)}{I_a I_j}} \tag{5}$$

However, in a system employing low impedance actuation, the zero's frequency can be an order of magnitude below the frequency of the flexible mode pole. This large separation amplifies the flexible mode peak by a factor approximately equal to the ratio of drive-link to motor inertias (see Figure 7).

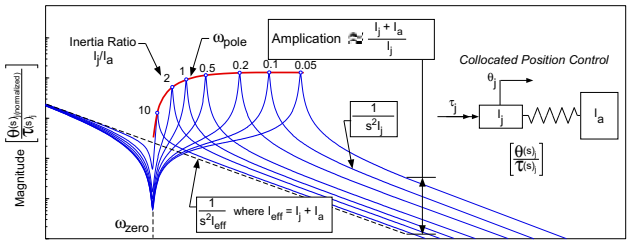


Figure 7: Open-loop transfer function of collocated motor position control: Amplification of oscillatory pole due to mismatched actuator-link inertia.

This effect severely limits the achievable closed-loop bandwidth and thus performance in general. The effect can be quite puzzling considering that the flexible mode frequency can be very high - an order of magnitude or more above the open-loop crossover frequency - and still cause excessive oscillations in the closed-loop response. Only when one considers the zero, whose frequency is affected by the larger driven-link inertia, does it become clear why the problem exists.

### 3.2.2 Achieving High Bandwidth Control

The challenge of implementing high bandwidth control in a DM$^2$ actuated system can be addressed through the combined implementation of prudent mechanical design techniques, which favorably modify the manipulator's open-loop dynamics, and control augmentation such as filtering and proper actuator-sensor placement.

In addition to mechanical modifications and control signal filtering[7], a somewhat surprising method to deal with the low frequency oscillations associated with low impedance actuation is to change the control topology from collocated to non-collocated control. We can understand this by examining the open-loop transfer function of a simple mass-spring model of an actuator-link system which employs non-collocated control. Figure 6b and Equation (4) show the assumed model and its associated transfer function. At first glance, this seems counter intuitive since in most cases the stabilizing effect of the zeros associated with collocated control is beneficial and allow for more aggressive gains. However, in the case of large inertia mismatch, the collocated control zero is the main cause of the problem. A comparison of peaking amplitude (see Figure 8) shows that for large mismatches the non-collocated control may be better than a collocated approach. Of course, this doesn't take into account the tendency of the oscillatory poles to become unstable, and special care must be taken to insure their stability, such as using of a notch filter or a gain stabilizing lag network[4, 3, 8]. With this consideration, we can conservatively assume that when using non-collocated control we can achieve a cross-over frequency as high as 1/5 of the flexible mode frequency. With this assumption, we can see from Figure 8 that when the high-frequency motor inertia is much less than the device inertia ($I_j/I_a < 10$) the use of non-collocated control allows for a higher closed-loop bandwidth than collocated control. The existing implementations of the DM$^2$ method, described in Section 4 have been implemented using the non-collocated approach.

## 4 Experimental Results

To evaluate the DM$^2$ actuation approach, a series of prototypes were built and evaluated, including a two degree-of-freedom (DOF) planar device and a three DOF spatial device (see Figures 9 and 10, respectively). The three DOF device incorporated many of the lessons learned with the evaluation of the two DOF device. As a result, the test results for the three DOF will show a marked improvement in performance. Both devices have relatively large workspaces (approximately 0.6 cubic meters).

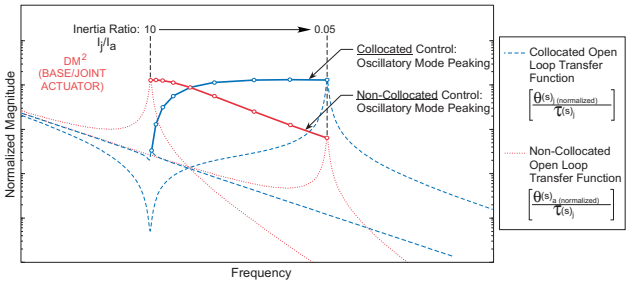


Figure 8: Variation of peaking amplitude for collocated and non-collocated position control for varying motor to load inertia ratios, $I_j/I_a$

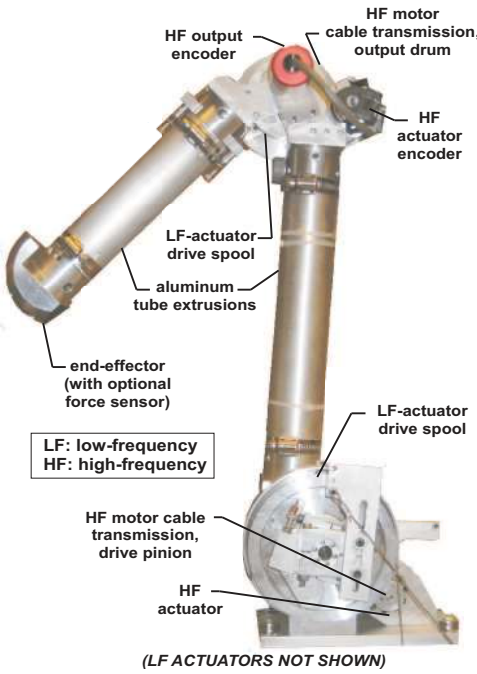


Figure 9: DM$^2$ two DOF prototype overview.

Numerous haptic-device performance metrics have been proposed [5, 12]. However, due to the inherent dynamic coupling between the device and user, it is difficult to obtain objective performance measurements [14]. Nevertheless, a simple set of haptic performance experiments were performed to evaluate the DM$^2$ approach and compare it to commercially available haptic devices.

End-effector haptic forces were experimentally measured using a six-axis force-torque sensor while end-effector position was determined using the forward kinematics of the manipulator with measured joint rotations. Desired haptic forces, $\mathbf{F_d}$, are realized through direct joint torque commands, $\tau_\mathbf{q}$. The required joint torques are calculated using the Jacobian associated with the end-effector linear velocity, $\mathbf{J_v}$.

$$\tau_\mathbf{q} = \mathbf{J_v^T F_d} \tag{6}$$

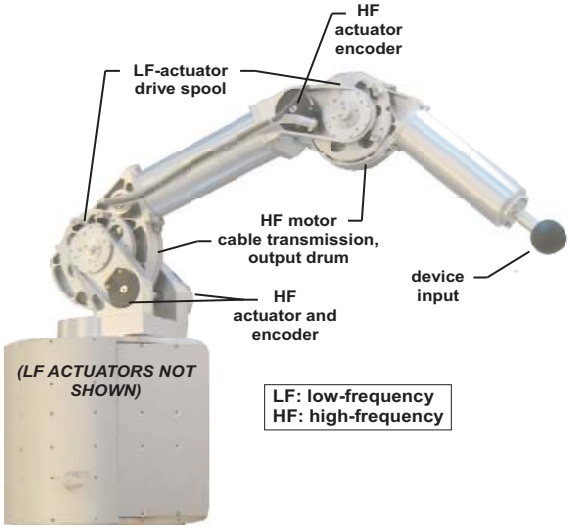


Figure 10: DM$^2$ three DOF prototype overview.

The required actuator torques are a function of the joint torques and drive-train kinematics. The calculation of the required actuator torque and subsequent control was implemented using a straightforward control structure [ref ZINN].

The first set of haptics performance experiments measured the maximum obtainable virtual wall stiffness. In each experiment, the virtual wall stiffness was increased until the device was no longer stable. As discussed earlier, the dynamic coupling between the device and the user makes it difficult to precisely define stability. For the purposes of this experiment, stability is defined as the point where the device requires noticeable effort on the part of the operator to prevent unwanted end-effector oscillations. Test results using both the two and three degree-of-freedom devices is shown in Figure 11. The plots in Figure 11 show measured end-effector force as a function of end-effector displacement perpendicular to the haptic virtual wall. The results plot the forces and displacement over approximately ten user interactions with the virtual wall.

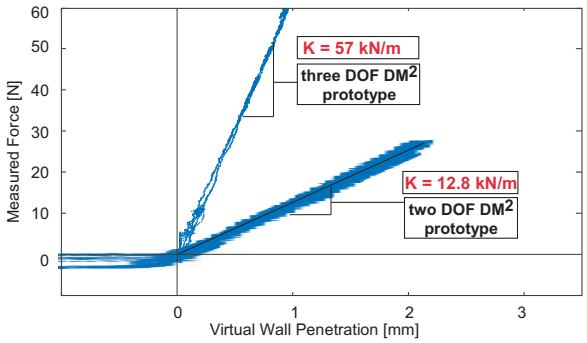


Figure 11: Maximum achievable virtual wall stiffness - measured end-effector force and displacement.

As seen in Figure 11, the maximum obtainable stiffness for the DM$^2$ two degree-of-freedom prototype was approximately 12 kN/m while the stiffness of the three degree-of-freedom device was in excess of 55 kN/m. In comparison to commercially available impedance-type haptic devices, the DM$^2$ actuated prototype has equal or greater stiffness (see Figure 12). In addition, the workspace volume of the two and three degree-of-freedom DM$^2$ prototypes are more than five times larger than the other devices listed in Figure 12[1]. Finally, the measured maximum continuous force of the two DOF DM$^2$ device is 50 percent larger than the commercial devices listed while the three DOF DM$^2$ device is more than 300 percent larger.

| Device / Specification | Delta | Omega | Phantom Premium 1.5 | Two DOF DM$^2$ | Three DOF DM$^2$ |
|---|---|---|---|---|---|
| Manufacturer | Force Dimension | Force Dimension | Sensable | Not Applicable | Not Applicable |
| Stiffness [N/mm] | 14.5 | 14.5 | 3.5 | 12.0 | 57.0 |
| Max Continuous Force [N] | 20 | 12 | 1.4 | 30 | 60 |
| Workspace Volume [ m$^3$] | 0.11 | 0.02 | 0.02 | 0.6 [a] | 0.6 |

[a] workspace volume based on two-dof testbed workspace with a hypothetical vertical third axis added

Figure 12: Haptic Device Comparison.

These results are summarized in Figures 13 and 14. As seen in Figures 13 and 14, the DM$^2$ implementation has increased the workspace, virtual stiffness, and maximum continuous force available as compared to the devices listed. The combination of all three characteristics are necessary for a successful large workspace haptic device implementation.

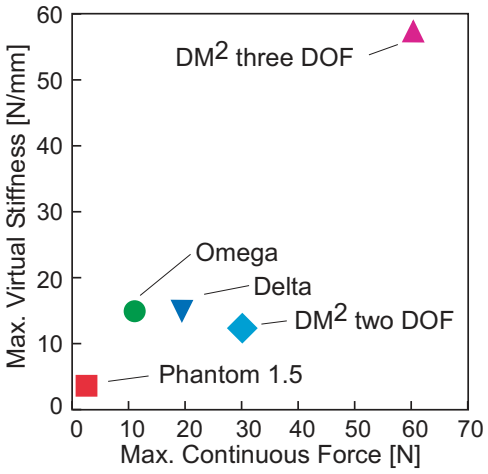


Figure 13: Maximum stiffness vs maximum continuous force (comparison of DM$^2$ prototypes to various commercial devices.

In addition to high stiffness and force output, haptic devices require low output impedance, as measured at the end-effector, to create the sense of transparency necessary to simulate zero force. Implementation of the DM$^2$ control structure described in Section 3 effectively removes the remaining low-frequency actuator friction and inertial forces not already attenuated by the low-frequency actuator SEA controller. To demonstrate this, a simple end-effector effective-friction experiment was carried out using the two-degree-of-freedom prototype. In the experiment, the end-effector was moved along a virtual line[2] and the forces at the end-effector were

[1]The workspace volume for the two DOF device in Figure 12 is based on the measured workspace area of the two-axis prototype with the addition of a hypothetical third axis, which is vertical and perpendicular to the two axes, and intersecting the center of the shoulder joint (joint 1) of the existing test-bed.

[2]Using hybrid control, where the end-effector was controlled to maintain

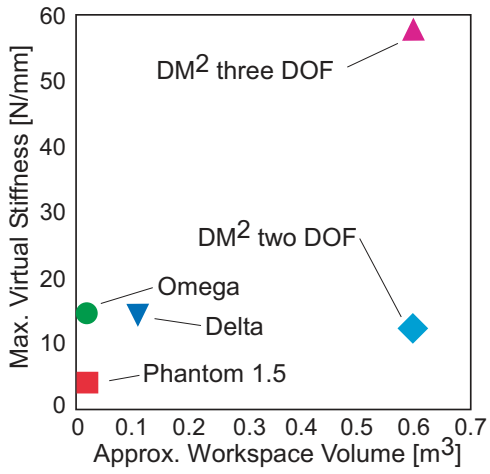


Figure 14: Maximum stiffness vs workspace (comparison of DM$^2$ prototypes to various commercial devices.

measured (see Figure 15). The measured forces are not a strong function of end-effector velocity and show a rectangular hysteresis loop, suggesting a coulomb-like friction source. As seen in Figure 15, the DM$^2$ approach is effective at eliminating the majority of device-friction (from its gear train and reflected rotor inertia), reducing the output friction to less than 1.5 Newtons.

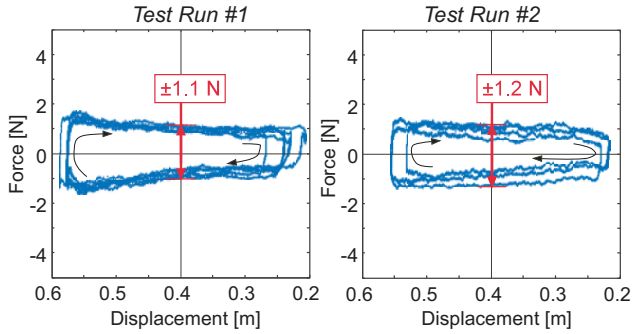


Figure 15: End-effector effective friction force as function of end-effector displacement.

## 5 Conclusion

We have presented the DM$^2$ actuation method in the context of a large workspace haptic device. Its qualifications in regards to transparency, performance and safety were discussed. The control scheme, simple in its design and implementation, was described along with some unique challenges that were overcome in its development. Experimental data showing the effectiveness of the approach was presented, demonstrating high overall stiffness, high force capability and low output impedance, all within a large workspace.

## Acknowledgements

This material is based upon work supported by the National Science Foundation under Grant No. EIA-9977717, the support of which is gratefully acknowledged.

its y-position while commanding zero force in the x-direction.

## References

[1] R. Adams, M. Moreyra, and B. Hannaford. Excalibur - a three axis force display. In *In Proceedings ASME International Mechanical Engineering Congress and Exhibition*, 1999.

[2] AMSE. *The PHANTOM Haptic Interface: A Device for Probing Virtual Objects*, Chicago, IL, 1994.

[3] R. H. Cannon and D. E. Rosenthal. Experiments in control of flexible structures with noncolocated sensors and actuators. *Journal of Guidance*, 7(5):546–553, 1984.

[4] R. H. Cannon and E. Schmitz. Initial experiments on the end-point control of a flexible one-link robot. *Intl. Journal of Robotics Research*, 3(3):62–75, 1984.

[5] J. E. Colgate and J. M. Brown. Factors affecting the z-width of a haptic display. In *Proc. IEEE Int. Conf. on Robotics and Automation*, pages 3205–3210, Las Alamitos, CA, 1994.

[6] R. V. der Linde, P. Lammertse, E. Frederiksen, and B. Ruiter. The hapticmaster, a new high-performance haptic interface. In *Proceedings of Eurohaptics02*, pages 1–5, Edinburgh, UK, 2002.

[7] G. Ellis and R. Lorenz. Resonant load control methods for industrial servo drives. In *Proc. of IEEE Industry Applications Society*, Rome, Italy, 2000.

[8] S. D. Eppinger and W. P. Seering. Three dynamic problems in robot force control. *IEEE Trans. on Robotics and Automation*, 8:751–758, Dec 1992.

[9] S. Grange, F. Conti, P. Rouiller, P. Helmer, and C. Baur. Review of the delta haptic device. In *Proceedings of Eurohaptics 2001*, Birmingham, England, July 2001.

[10] V. Hayward and O. Astley. Performance measures for haptic interfaces. In G. Giralt and G. Hirzinger, editors, *Robotics Research: The 7th International Symposium*, pages 195–207. Springer Verlag, 1996.

[11] O. Khatib. Reduced effective inertia in macro-mini-manipulator systems. In H. Miura and S. Arimoto, editors, *Robotics Research 5, Proc. 5th Int. Symposium*, pages 279–284, Cambridge, MA, 1990. MIT Press.

[12] D. A. Lawrence, L. Y. Pao, A. M. Dougherty, M. A. Salada, and Y. Pavlou. Rate-hardness: A new performance metric for haptic interfaces. *IEEE Trans. on Robotics and Automation*, 16(4):357–371, August 2000.

[13] J. Morrel. *Parallel Coupled Micro-Macro Actuators*. PhD thesis, Massachusetts Institute of Technology, Cambridge, MA, 1996.

[14] J. B. Morrell and J. K. Salisbury. Performance measurements for robotic actuators. In *Proc. ASME Int. Mechanical Engineering Congress and Exposition*, page 531528, Atlanta, GA, November 1996.

[15] G. Pratt and M. Williamson. Series elastic actuators. In *Proc. of IEEE/RSJ International Conference on Intelligent Robots and Systems*, volume 1, pages 399–406, Pittsburgh, PA, 1995.

[16] D. Robinson. *Design and Analysis of Series Elasticity in Closed-loop Actuator Force Control*. PhD thesis, Massachusetts Institute of Technology, Cambridge, MA, June 2000.

[17] S. J. Schroeck and W. C. Messner. On compensator design for linear time-invariant dual-input single-output systems. *IEEE Transactions on Mechatronics*, 6(1):50–57, March 2001.

[18] W. Townsend. *The Effect of Transmission Design on Force-Controlled Manipulator Performance*. PhD thesis, Massachusetts Institute of Technology, Cambridge, MA, April 1988. AI-TR 1054.

[19] M. Ueberle and M. Buss. Design, control, and evaluation of a new 6 dof haptic device. In *In Proceedings of the 2002 IEEE/RSJ International Conference on Intelligent Robots and Systems*, page 29492954, 2002.

[20] M. Zinn. *A New Actuation Approach For Human Friendly Robotic Manipulation*. PhD thesis, Stanford University, Stanford, CA, August 2005.

[21] M. Zinn, O. Khatib, B. Roth, and J. Salisbury. A new actuation approach for human friendly robot design. *Int. J. of Robotics Research*, 23(4/5):379–398, April-May 2002.